Entraining Flow of a Concentrated Benthic Suspension. Computations with the Prandtl Mixing-Length Model

C. Kranenburg

Report No. 3 - 99

Prepared for the European Commission, DG XII
MAST3 - COSINUS Project
Contract No. MAS3-CT97-0082

1999

TU Delft
Technische Universiteit Delft

Faculteit der Civiele Techniek

Entraining Flow of a Concentrated Benthic Suspension. Computations with the Prandtl Mixing-Length Model

C. Kranenburg

Report No. 3 - 99

Prepared for the European Commission, DG XII
MAST3 - COSINUS Project
Contract No. MAS3-CT97-0082

1999

Delft University of Technology
Faculty of Civil Engineering and Geosciences
Hydromechanics Section

Abstract

The Prandtl mixing-length model of turbulent exchange of mass and momentum is applied to calculate the entrainment of overlying water into a layer of suspended fine sediment at a horizontal bed. In the field the flow and turbulence in such a concentrated benthic suspension (CBS) are driven by a streamwise pressure gradient resulting from the tide. However, in this report a proposed laboratory experiment is simulated in which flow and turbulence in the CBS are driven by a movable bottom screen which is started instantaneously from rest. The aims of the calculations are to show the feasibility of this laboratory experiment, to carry out a sensitivity analysis and, in future work, to compare with experimental results. Damping functions accounting for the reduction in turbulent exchange caused by density stratification are calibrated using results of entrainment experiments with two-fluid systems reported in the literature. The adopted model of the rheological behaviour of the CBS is of the Herschel-Bulkley type. In addition, the effects of hindered settling and sidewall friction are included. Entrainment rates are found to be particularly sensitive to the speed of the screen and the excess weight of the sediment, whereas the rheological model has little influence.

Contents

1 Introduction

Suspended fine sediments in tidal waters may be deposited during slack water periods to form a mud layer, also designated in the literature as a (high-)concentrated benthic suspension (CBS), on a more permanent bed. When after slack water the tide strengthens, the associated streamwise pressure gradient causes the CBS layer to flow with the overlying water layer. In the CBS layer turbulence is generated by bed friction, as a result of which water is entrained into this layer so that the depth of the CBS layer gradually increases and the sediment concentration decreases. If the water depth is not too large, the sediment will get mixed across the whole water column after some time.

On a larger time scale, a similar process may occur during the neap-tide spring-tide cycle. Mud deposited during neap-tide then is mixed across the water depth, or part of it, during spring tide.

When the mud has deposited, the process of self-weight consolidation commences at concentrations beyond the gelling value. Pore water is expelled, concentrations increase and a bed structure develops. As a result a yield strength develops, first at the base of the mud layer and later on also at higher levels. A non-zero yield strength implies that, during acceleration of the tidal flow, only the part of the mud layer starts to flow in which the tide-induced shear stress is larger than the yield stress. This (upper) part of the mud layer is a CBS, whereas the part that does not flow behaves as a soil.

On the relatively small time scale of the tidal cycle the developed yield strength may be small so that the entrainment process described is likely to dominate. However, in the case of the neap-tide spring-tide cycle sufficient time is available during neaps for the yield strength to become large so that the classical erosion process as described by Partheniades (1965) will take place.

The entrainment process described has received little attention (Kranenburg and Winterwerp 1997, Winterwerp 1999). For this reason a laboratory entrainment experiment is to be carried out as part of the EC-MAST3 COSINUS Project, which deals with cohesive sediment transport and processes in the bed. This experiment will be carried out in the annular flume of the Delft University of Technology. Contrary to the situation in the field, flow and turbulence in the CBS layer are produced by a rotating bottom screen on which the mud had deposited when the screen was at rest, see Figure 1 and Kranenburg and Bruens (1998).

The aims of the work reported herein are to develop a mathematical model of the entrainment experiment to be conducted in the laboratory, to show that the experiment is feasible and to carry out a sensitivity analysis. In future work the mathematical model, which can be easily adapted to tidal-flow conditions, will be validated with data obtained from the experiment.

Mathematical modelling of the entrainment process requires a rheological model of the CBS and a turbulence model. For this purpose a Herschel-Bulkley type of model and the Prandtl mixing-length (PML) model are adopted, respectively. The bed (the bottom screen) is assumed to be horizontal and the flow is uniform. These simplifications allow a one-dimensional model to be used.

The mathematical model is described in Section 2 of this report. Results of numerical simulations of the experiment mentioned are presented in Section 3. Conclusions from this work are drawn in Section 4.

2 One-dimensional entrainment model

2.1 Mean-flow equations

The flow considered is a uniform free-surface flow of water and CBS over a horizontal bottom screen. A study of Spalding and Svensson (1977) indicates that ignoring any rotational effects as occurring in annular flumes does not seriously affect the entrainment modelling. Therefore, the effects of rotation are neglected.

Adopting the Bousinesq approximation for small density differences, the equation of motion in the direction of the flow becomes

$$\frac{\partial U}{\partial t} \approx \frac{\partial}{\partial z}\left(\nu \frac{\partial U}{\partial z} - \langle uw \rangle\right) - \frac{2}{\rho_w}\frac{\tau_w}{B} \tag{2.1}$$

where U = U(z,t) is the averaged flow velocity of water and CBS, t time, z the vertical coordinate (positive upward, z = 0 at the screen), ρ_w the density of the water, ν the kinematic viscosity of the CBS, <uw> the turbulent shear stress, τ_w the sidewall friction and B the width of the flume.

The mass balance equation for the sediment reads

$$\frac{\partial C}{\partial t} = \frac{\partial}{\partial z}\left(W_s C - \langle wc \rangle\right) \tag{2.2}$$

where C = C(z,t) is the averaged sediment concentration, W_s the settling velocity and <wc> the vertical turbulent mass transport. As the primary cohesive particles form larger flocs, molecular diffusion of the sediment is negligible.

The kinematic viscosity of the CBS is modelled according to a Herschel-Bulkley type of expression,

$$\nu = \nu_w\left[1 + p\left(\frac{C}{\rho_s}\right)^q\left(\frac{|\partial U/\partial z|_0}{|\partial U/\partial z|}\right)^r\right] \tag{2.3}$$

where ν_w is the kinematic viscosity of the water, ρ_s the density of the sediment, $|\partial U/\partial z|_0$ is a reference shear rate (= 1 s^{-1}), and p, q and r are positive coefficients. Thixotropic effects are not accounted for by (2.3).

The dependence of the viscosity on the velocity gradient represents the shear-thinning behaviour of mud suspensions. The influence of turbulent shear is not explicitly taken into account in (2.3), but is probably not negligible. The appropriate shear-rate parameter for turbulence is $G = (\epsilon/\nu)^{1/2}$, where ϵ is the dissipation rate. In the case of local equilibrium of the turbulence, which is also assumed in the PML model, ϵ is equal to the turbulence production, $\langle uw \rangle \partial U/\partial z = \nu_T(\partial U/\partial z)^2$, where ν_T is the eddy viscosity. The parameter G then becomes equal to $(\nu_T/\nu)^{1/2}|\partial U/\partial z|$. A requirement for the flow to be turbulent is that $\nu_T/\nu \gg 1$ (e.g., $\nu_T/\nu > 15$). This means that in turbulent local-equilibrium shear flow G is always larger than $|\partial U/\partial z|$. In (2.3) this effect is absorbed in the parameter p. The sensitivity of results to this parameter is discussed in Section 3.2.

As only suspensions are considered, consolidation and the build-up of a yield strength

prior to an experiment are beyond the scope of this report. If strength develops, it will start to do so at the screen. The underlying assumption therefore is that the applied shear stress at the screen is larger than the yield stress. As is shown in Section 3, the shear rates near the screen in case a flow is generated are large so that viscous shear stress is dominant and some strength has little influence.

Sidewall friction is modelled as usual for turbulent flow,

$$\tau_w = \rho_w \lambda U^2 \qquad (U \geq 0) \tag{2.4}$$

where λ is a friction coefficient given by a formula of the Blasius type (Kranenburg and Winterwerp, 1997).

The effect of hindered settling on the settling velocity is modelled according to Ross and Mehta (1989),

$$W_s = W_0 \left(1 - \frac{C}{C_{gel}} \right)^5 \tag{2.5}$$

where W_0 is the settling velocity of a single floc and C_{gel} the gelling concentration.

Water, sediment and screen are assumed at rest before an experiment is started. The initial conditions (at t = 0) therefore are given by

$$U(z,0) = 0 \tag{2.6}$$

$$C(z,0) = C_0(z) \tag{2.7}$$

The boundary conditions at the free surface (z = h) are

$$\langle uw \rangle (h,t) = 0 \tag{2.8}$$

$$C(h,t) = 0 \tag{2.9}$$

Equation 2.9 ensures that the transport caused by settling vanishes at z = h; it follows from (2.8) and the turbulence model presented in Section 2.2 that $\partial U(h,t)/\partial z = 0$, and hence from (2.13) presented in Section 2.2 that, as required, $\langle wc \rangle (h,t) = 0$.

The boundary conditions at the screen (z = 0) are the standard conditions for flow past a smooth wall, and a zero sediment transport,

$$U(z,t) = U_s - \frac{u_*}{\kappa} \ln\left(1 + \frac{z}{z_0}\right) \qquad (z \to 0) \tag{2.10}$$

$$W_s C(0,t) - \langle wc \rangle (0,t) = 0 \tag{2.11}$$

where $U_s = U_s(t)$ is the speed of the screen ($U_s(0) = 0$), u_* the friction velocity, κ Von Karman's constant ($\kappa = 0.41$) and z_0 a viscous length scale, $z_0 = 0.11\nu(0,t)/u_*(t)$.

2.2 Turbulence model

The PML model gives the vertical transports of momentum and mass as (e.g., Rodi, 1980)

$$\langle uw \rangle = - l^2(z,t) \left|\frac{\partial U}{\partial z}\right| \frac{\partial U}{\partial z} F(Ri) \tag{2.12}$$

$$\langle wc \rangle = - \frac{1}{\sigma_{T0}} l^2(z,t) \left|\frac{\partial U}{\partial z}\right| \frac{\partial C}{\partial z} G(Ri) \tag{2.13}$$

where $l(z,t)$ and σ_{T0} are mixing-length and turbulent Prandtl-Schmidt number under neutral conditions, and F(Ri) and G(Ri) are damping functions accounting for the reduction in turbulent exchange caused by density stratification. The gradient Richardson number Ri is defined as

$$Ri = - \frac{\Delta g}{\rho_w} \frac{\partial C}{\partial z} \left(\frac{\partial U}{\partial z}\right)^{-2} \tag{2.14}$$

where $\Delta = (\rho_s - \rho_w)/\rho_s$.

The flow of CBS as shown in Figure 1 can be classified as a turbulent wall boundary-layer flow. The mixing-length distribution in such a flow can be approximated, in the case of negligible stratification and high Reynolds numbers, by a ramp function given by (e.g., Cebeci and Bradshaw, 1977)

$$l = \kappa z \qquad (0 \leq z \leq \theta H) \tag{2.15}$$

$$l = \theta H \qquad (\theta H < z \leq H) \tag{2.16}$$

where H is the depth of the turbulent CBS layer and θ a coefficient, $\theta = 0.20 \pm 0.02$. The value adopted herein is $\theta = 0.20$.

Equation 2.16 indicates that in the domain $\theta H < z \leq H$ the mixing length increases as H increases during the entrainment process. This means that in a numerical model of this process the depth H has to be determined as a function of time. A simpler approach would be to replace H in (2.15) and (2.16) by the water depth h, which is constant. However, in this way turbulent exchange is overestimated and the entrainment rate, dH/dt, becomes too large. It is shown in the Appendix that, in the case where $H < \theta h$ and stratification is negligible, the simpler approach yields an entrainment rate that is too large by a factor of about three. However, the error is less when stratification suppresses the turbulence and thus reduces the effective mixing length.

The depth H(t) of the CBS layer is defined herein as the level at which the difference of the concentration at time t from the initial concentration equals the concentration at the screen multiplied by a factor of 0.001,

$$|C[H(t),t] - C_0[H(t)]| = 0.001\,C(0,t) \tag{2.17}$$

Results were found to be insensitive to variation of this factor provided it was much less than one. An additional condition is $dH/dt \geq 0$.

It is well known from the literature that the damping functions in the PML model are far from universal. In particular, these functions differ for free turbulence and wall turbulence. In free turbulence the direct influence of rigid boundaries on the turbulence structure is minor, whereas this influence is dominant in wall turbulence. The damping functions adopted in an earlier report (Kranenburg, 1998) apply exclusively to free turbulence. These functions read, for eddy viscosity and eddy diffusivity, respectively,

$$F(Ri) = \frac{1}{(1 + 2.4Ri)^2} \tag{2.18}$$

$$G(Ri) = \frac{1}{(1 + 2.4Ri)^4} \tag{2.19}$$

An example of flows in which wall turbulence prevails is the atmospheric surface layer. In this case the turbulence damping is stronger than suggested by (2.18) and (2.19). A well-known expression representing this stronger damping is the Monin-Obukhov relation, which can be written as $F(Ri) = (1 - \beta Ri)^2$, in which $0 \leq Ri \leq 1/\beta$. Empirical values of the coefficient β range from 5 to 10 with $\beta \approx 7$ as the most likely value (e.g., Rodi, 1980). However, it is also known that this relation overestimates damping in the case of strong stratification, that is, for values of Ri near $1/\beta$ (e.g., Turner, 1973). To accommodate the damping function F(Ri) to this fact an exponential function is proposed herein,

$$F(Ri) = \exp(-\alpha Ri) \tag{2.20}$$

in which α is an empirical coefficient. Comparison with the Monin-Obukhov relation shows that α should be about 2β, that is, $\alpha \approx 14 \pm 4$. The coefficient α is determined for the present application in Section 2.3.

The turbulent Prandtl-Schmidt number σ_T in stratified wall flows, where $\sigma_T = \sigma_{T0}F/G$, varies much less with Ri than in free turbulence. However, because of experimental scatter, it is difficult to devise a functional relationship between σ_T and Ri. Arya (1972) reported values ranging from 1.4 to 1.7 for Ri larger than 0.03. Gartrell (1979) found values of σ_T between one and about two, but again the scatter was large. For this reason, and because entrainment rates are influenced mainly by the value of σ_T for near-collapsing turbulence, it is assumed that σ_T is constant ($= \sigma_{T0}$). The adopted value of σ_T is 1.5, which is about the mean value of the figures mentioned. As a consequence of a constant σ_T, the damping functions F and G become the same,

$$G(Ri) = F(Ri) = \exp(-\alpha Ri) \tag{2.21}$$

2.3 Calibration of damping functions

The coefficient α in (2.21) is determined using experimental data from entrainment experiments with a two-fluid system reported in the literature. For this purpose the settling velocity is equated to zero, sidewall friction is dropped, the viscosity is equated to that of the fluids (water), and the lower layer is the denser layer. The bottom screen is started instantaneously and its speed kept constant afterwards.

Laboratory experiments corresponding to this simplified case were carried out for the first time by Kantha et al. (1977)[1]. However, the results of those authors were much influenced by sidewall fricton. Price (1979) and Thompson (1979) independently described methods to correct for this effect, and found that for sufficiently strong stratification the entrainment rate dH/dt is given by an expression of the form

[1]In most entrainment experiments, including those of Kantha et al., a shear stress is exerted at the top of the water column so that the upper layer is the entraining layer.

$$\frac{1}{u_*}\frac{dH}{dt} \approx \frac{k}{Ri_*^{1/2}} \tag{2.22}$$

where k is a constant, k ≈ 0.6 (Price) to about 0.9 (Thompson), and Ri_* is a bulk Richardson number given by $Ri_* = w/(\rho_w u_*^2)$. Here w is the total excess weight of the lower layer which in the present case is given by

$$w = \Delta g \int_0^{H_0} C_0(z)\, dz \tag{2.23}$$

Kranenburg (1984) carried out laboratory experiments in which sidewall friction was compensated for, and obtained results that approximately agree with (2.22) for Ri_* larger than about 20 and $k = 0.6 \pm 0.1$. These experiments were simulated with the present PML model. Figure 2 shows a comparison between calculated and measured entrainment rates, both determined using the maximum-gradient method[2], for $\alpha = 12$. The agreement with the measurements is excellent. The results, both experimental and theoretical, show a small but significant deviation from the $Ri_*^{-1/2}$ behaviour given by (2.22).

Some calculations were also made with $\alpha = 15$. In this case both dH/dt and u_* were less so that a curve slightly below that in Figure 2 was obtained. Because the friction velocities at the bottom screen were realistic for $\alpha = 12$, and too low for $\alpha = 15$, all further calculations were carried out with $\alpha = 12$.

Kranenburg (1984) measured density distributions, which can be used to check, to some extent, the assumed value of σ_T. Figures 3a and 3b show results obtained with the present mathematical model. The water depth is 0.3 m, the speed of the screen is 0.5 m/s and the excess weight given by (2.23) is 30.2 N/m^2. All concentration distributions in Figure 3a for $\sigma_T = 1.5$ show an inflection point, whereas those in Figure 3b for $\sigma_T = 1$ do not. Because all measured density distributions also showed inflection points, the value $\sigma_T = 1.5$ is the more realistic one.

For comparison, Figure 3c shows results obtained with the damping functions for free turbulence given by (2.18) and (2.19). In this case the calculated concentration distributions are completely at variance with the measurements, which yielded distributions closely resembling those of Figure 3a.

Comparing Figures 3a and 3b, it is seen that for a fixed value of α the entrainment rates are less for the larger σ_T (which is not surprising because the eddy diffusivity decreases for increasing σ_T). Therefore the calibrated value of α depends on the value of σ_T selected.

---

[2]A tangent is drawn through the inflection point in the concentration distribution at time t; the point of intersection of the tangent with the vertical axis gives the layer depth H(t).

3 Numerical computations

3.1 Cases examined

The equations presented in Section 2 were solved numerically to examine entraining flows of CBS, and to provide a theoretical basis for the laboratory experiment referred to in the Introduction. The numerical scheme used was the explicit Euler scheme and the grid was equidistant. The assumed values of the various parameters involved are representative of the laboratory experiment. The water depth above the screen is 0.25 m, the width of the flume is 0.30 m, the densities of water and sediment are 1000 and 2600 kg/m^3, the kinematic viscosity of the water is 10^{-6} m^2/s and the settling velocity is put at 2×10^{-4} m/s. The initial distribution of the sediment concentration is given by

$$C_0(z) = C_t + (C_{gel} - C_t)\left(1 - \frac{z}{H_0}\right)^2 \qquad (3.1)$$

where $H_0 = H(0)$, $C_{gel} = C(0,0)$ and $C_t = C(H_0, 0)$. The assumed values of these parameters are listed in Table 3.1 together with those of the speed of the screen U_s and the rheological parameter r in (2.3). The rheological parameters p and q are put at 10^6 and 3, which values correspond, to an order of magnitude, to values measured by De Wit (1995) and Berlamont and Van Goethem (1984).

Table 3.1. *Computational runs. Values differing from those of Run 1 are underlined.*

Run No.	H_0 (m)	C_{gel} (kg/m^3)	C_t (kg/m^3)	U_s (m/s)	r -
1	0.05	150	100	0.90	0.8
2	0.05	150	100	0.60	0.8
3	0.05	150	100	1.20	0.8
4	0.05	150	100	0.90	0
5	0.05	200	150	0.90	0.8
6	0.10	150	100	0.90	0.8

As stated before, the bottom screen is started instantaneously from rest (at t = 0) and its speed remains constant afterwards. The boundary conditions are given by (2.8) through (2.11). The time step and grid size are 0.002 s and h/100. This grid size is sufficiently small for the solutions to converge[3].

3.2 Results

The results of Run 1 shown in Figure 4 indicate that, as discussed before, the entrainment process causes the depth of the CBS layer to increase, and concentrations to decrease. However, the entrainment rate (dH/dt) decreases for larger times, mainly because of sidewall friction. The influence of sidewall friction, which reduces flow velocities and therefore entrainment rates, increases with time because the depth of the flowing layer increases. An increase in settling velocity also reduces entrainment rates, but this effect was found to be of minor importance because of hindered settling.

As in the case of the two-fluid system dealt with in Section 2.3, density stratification greatly reduces entrainment rates. Although the flow near the bottom screen is virtually unstratified, stratification is strong at the entraining interface (the lutocline).

In some cases a more or less steady-state final situation was obtained with the CBS layer depth less than the water depth. Figure 4 also shows this tendency.

Figures 5 and 6 (Runs 2 and 3) show the strong influence of the speed of the screen. Hardly any mixing seems to occur for $U_s = 0.60$ m/s, whereas complete mixing is found for $U_s = 1.20$ m/s. In Run 2 the mixing may even be overestimated, because the calculated depths of the CBS layer (as indicated by the dashes on the left of the vertical axis) seem quite large. This may have led to an overestimation of the mixing length.

Figure 7 shows the results of Run 4, in which the shear-thinning behaviour of the viscosity was omitted (r = 0). Near the screen, where the shear rates are largest (about 120 s^{-1}), the viscosity now is large initially. The higher viscosity causes higher entrainment rates because momentum is more easily transferred in the upward direction, but this effect diminishes in later stages as concentrations decrease.

It may be questioned in the case of Run 4 whether the flow in the CBS layer should become turbulent. The initial kinematic viscosity at the screen is 1.9×10^{-4} m^2/s and the friction velocity is 0.15 m/s. The thickness of the viscous sublayer, which is about $10\nu/u_*$, then becomes 0.013 m. As the initial depth of the CBS layer is 0.05 m, this layer will become turbulent for the larger part. However, a low-Reynolds number extension of the PML model, e.g. the Van Driest model, would be needed to obtain correct results, the more so because the grid size is only 0.0025 m. It is noted that the low-Reynolds-number problem only exists initially. At $t \approx 100$ s the kinematic viscosity has decreased to a value for which the thickness of the viscous sublayer no longer exceeds the grid size. This problem does not exist either in the more realistic case where r is around 0.8.

The results are very sensitive to a reduction of the parameter q, because the viscosity then may become extremely large. However, if p and q are varied simultaneously so that the viscosity retains realistic values, the results change little. For example, the combinations $(p,q) = (6 \times 10^4, 2)$ and $(p,q) = (1.8 \times 10^7, 4)$, both give $\nu \approx 2 \times 10^{-4}$ m^2/s for C = 150

---

[3]The numerical model was also tested by comparing results for a homogeneous fluid with the analytical solution given in the Appendix. The computed dimensionless entrainment rate is 0.315 ± 0.010, in agreement with the analytical result.

kg/m^3 and $|\partial U/\partial z| = 1\ s^{-1}$, and yield almost the same results as those of Run 1.

The turbulence-induced shear, which is discussed in Section 2.1, effectively reduces the parameter p in (2.3). However, even equating this parameter to zero, that is, putting $\nu = \nu_w$, yields results that differ little from those of Run 1. The depth of the CBS layer at t = 50 s is less by 3 percent, but for larger times differences are hardly distinguishable.

Higher initial concentrations reduce the entrainment rates, because more work has to be done against gravity to transport the sediment upward. An example is shown in Figure 8 (Run 5).

Finally, Figure 9 (Run 6) shows the influence of a thicker CBS layer. The results are similar to those of Figure 5 (Run 2), which is not surprising. In Run 2 the input of kinetic energy is reduced, with respect to Run 1, by a factor of about $(0.60/0.90)^2 \approx 0.44$, and in the case of Run 6 the work to be done is larger than in Run 1 by a factor 2. The overall Richardson numbers Ri_* for Runs 2 and 6 therefore do not differ so much.

4 Conclusions

The following conclusions can be drawn from this work:

1. The distribution of the mixing-length in the PML model should be adapted to the depth of the turbulent (CBS) layer, in particular if stratification is weak.
2. The computations made support the finding reported in the literature that the damping functions in the PML model are different for free turbulence and wall turbulence. In the latter case the Prandtl-Schmidt number varies considerably less with the gradient Richardson number. The exponential damping functions proposed yield satisfactory results for two-fluid systems.
3. The numerical results indicate that the laboratory experiment referred to in the Introduction and Section 3.1 is feasible in that turbulent entrainment and mixing seem to occur at realisable speeds of the bottom screen.
4. The computational results for the laboratory experiment are sensitive to the speed of the bottom screen and the excess weight of the CBS. The results are quite insensitive to settling velocity, and to the rheological parameters p, q and r provided that the viscosity does not become unrealistically large. Even equating parameter p to zero to account for floc break-up by turbulent shear hardly influences the results.
5. Application of the mathematical model developed to field situations has to be preceded by validation with data from the laboratory experiment simulated.

Acknowledgements

The author is grateful to Mr. A.M. den Toom of the Laboratory of Hydromechanics, who implemented the numerical model. This work was carried out as part of the MAST3-COSINUS Project. It was partially funded by the European Commission, Directorate General XII, under Contract No. MAS3-CT97-0082.

References

Arya, S.P.S. (1972) The critical condition for the maintenance of turbulence in stratified flows. *Quart. J. R. Met. Soc.* **98**, 264-273.

Berlamont, J. and J. van Goethem (1984) Prevention of mud accumulation in harbours and their entrances. *Research Report to SBBM.* Katholieke Universiteit Leuven, Belgium (in Dutch).

Cebeci, T. and P. Bradshaw (1977) *Momentum Transfer in Boundary Layers.* Hemisphere Publ. Corp., Washington, London.

De Wit, P.J. (1995) *Liquefaction of Cohesive Sediments Caused by Waves.* Ph. D. Thesis, Delft University of Technology, the Netherlands.

Gartrell, G. Jr. (1979) Studies on the mixing in a density stratified shear flow. *Report No. KH-R-39.* California Institute of Technology, U.S.A.

Kantha, L.H., O.M. Phillips and R.S. Azad (1977) On turbulent entrainment at a stable density interface, *J. Fluid Mech.* **79**, 753-768.

Kranenburg, C. (1984) Wind-induced entrainment in a stably stratified fluid. *J. Fluid Mech.* **145**, 253-273.

Kranenburg, C. (1998) Saturation concentrations of suspended fine sediment. Computations with the Prandtl mixing-length model. *Report No. 5-98.* Delft University of Technology, the Netherlands.

Kranenburg, C. and J.C. Winterwerp (1997) Erosion of fluid mud layers. I: Entrainment model. *J. Hydraul. Engrg* **123**, 504-511.

Kranenburg, C. and A.W. Bruens (1998) A flume experiment on CBS dynamics. In: *Book of Abstracts*, MAST3-COSINUS Annual General Meeting, Grenoble (E.A. Toorman and J.E. Berlamont, eds.). Katholieke Universiteit Leuven, Belgium.

Partheniades, E. (1965) Erosion and deposition of cohesive soils. *J. Hydraul. Div.* **91**, 105-139.

Price, J.F. (1979) On the scaling of stress-driven entrainment experiments. *J. Fluid Mech.* **90**, 509-529.

Rodi, W. (1980) *Turbulence Models and their Application in Hydraulics.* International Association for Hydraulic Research, Delft, the Netherlands.

Ross, M.A. and A.J. Mehta (1989) On the mechanics of lutoclines and fluid mud. *J. Coastal Res.* Special Issue No. 5, 51-62.

Spalding, D.B. and U. Svensson (1977) The development and erosion of the thermocline. In: *Heat Transfer and Turbulent Buoyant Convection* (D.B. Spalding and N. Afgan, eds.) **1**, 113-122. Hemisphere Publ. Corp., Washington, London.

Tennekes, H. and J.L. Lumley (1972) *A First Course in Turbulence.* MIT Press, Cambridge, U.S.A.

Thompson, R.O.R.Y. (1979) A reinterpretation of the entrainment process in some laboratory experiments. *Dyn. Atmos. Oceans* **4**, 45-55.

Turner, J.S. (1973) *Buoyancy Effects in Fluids.* Cambridge University Press, Cambridge, U.K.

Winterwerp, J.C. (1999) *On the Dynamics of High-Concentrated Mud Suspensions.* Ph.D. Thesis, Delft University of Technology, the Netherlands (to appear).

Appendix - Analytical solution for a homogeneous fluid

The equations presented in Section 2 can be solved analytically in the special case where:

- The shear stress at the bottom screen is constant.
- Viscous effects are negligible.
- Sidewall friction is absent.
- Density stratification is absent.

The last condition is not a necessary one, but is introduced herein for the sake of convenience. It implies that the coupling between momentum equation (2.1) and the mass balance (2.2) is dropped.

The momentum equation (2.1) together with the PML model (2.12) now can be written as

$$\frac{\partial U}{\partial t} = \frac{\partial}{\partial z}\left[l^2(z,t) \left| \frac{\partial U}{\partial z} \right| \frac{\partial U}{\partial z} \right] \tag{A.1}$$

This equation allows a similarity solution of the form $U = U(\eta)$, where η is given by

$$\eta = \frac{z}{H(t)} \tag{A.2}$$

Substituting from (A.2), Equation A.1 becomes

$$w_e \eta U' + \frac{\mathrm{d}}{\mathrm{d}\eta}\left[\frac{l^2(z,t)}{H^2(t)} |U'| U' \right] = 0 \tag{A.3}$$

where $w_e = dH/dt$ is the entrainment rate and $U' = dU/d\eta$. Equations 2.15 and 2.16 show that the mixing-length $l(z,t)$ can be written as $l(z,t) = H(t)\phi(\eta)$, where ϕ is a known function of η. Equation A.3 thus can be written, for $U' < 0$,

$$w_e \eta - 2\phi(\eta) \frac{\mathrm{d}}{\mathrm{d}\eta}[\phi(\eta) U'] = 0 \tag{A.4}$$

This result shows that in the case of similarity the entrainment rate is constant.

Equation A.4 can be integrated once to give

$$\phi U' = \frac{1}{2} w_e \int_0^{\eta} \frac{\eta_1 \, d\eta_1}{\phi(\eta_1)} + c_1 \tag{A.5}$$

where the integration constant c_1 is determined from the boundary condition (2.8) for the shear stress at z = H, that is, at $\eta = 1$. As the shear stress is proportional to $(\phi U')^2$, Equation (A.5) becomes

$$\phi U' = -\frac{1}{2} w_e \int_{\eta}^{1} \frac{\eta_1 \, d\eta_1}{\phi(\eta_1)} \tag{A.6}$$

At the screen (z = 0), the relationship $\langle uw \rangle(0,t) = u_*^2$ gives $-\phi(0)U'(0) = u_*$. Substituting from (A.6) then gives

$$E_* \int_0^1 \frac{\eta \, d\eta}{\phi(\eta)} = 2 \tag{A.7}$$

where $E_* = w_e/u_*$ is a dimensionless entrainment rate. Equation A.7 shows that E_* is proportional to the dimensionless mixing-length ϕ.

Adopting the mixing-length distribution given by (2.15) and (2.16), the integral in (A.7) can be evaluated to give

$$E_* = 4\kappa \frac{\theta}{1 + \theta^2} \tag{A.8}$$

Substituting the values of κ and θ selected in Section 2.2, that is, $\kappa = 0.41$ and $\theta = 0.20$, the dimensionless entrainment rate becomes $E_* = 0.31$, somewhat larger than the value of 0.28 Tennekes and Lumley (1972) derived from experimental data.

If a mixing-length distribution for turbulence in the whole water column is prescribed, the mixing-length in a shallow CBS layer ($H/h \ll 1$, which is usually true in the field) then is given by $l \approx \kappa z$. This case corresponds with a value of θ equal to one so that the dimensionless entrainment rate becomes $2\kappa = 0.82$. Neglecting the fact that only the CBS layer is turbulent, and its consequenses for the mixing-length distribution, therefore results in an entrainment rate that is too high by a factor of almost three. It is noted that this result applies to the unstratified case.

FIGURES

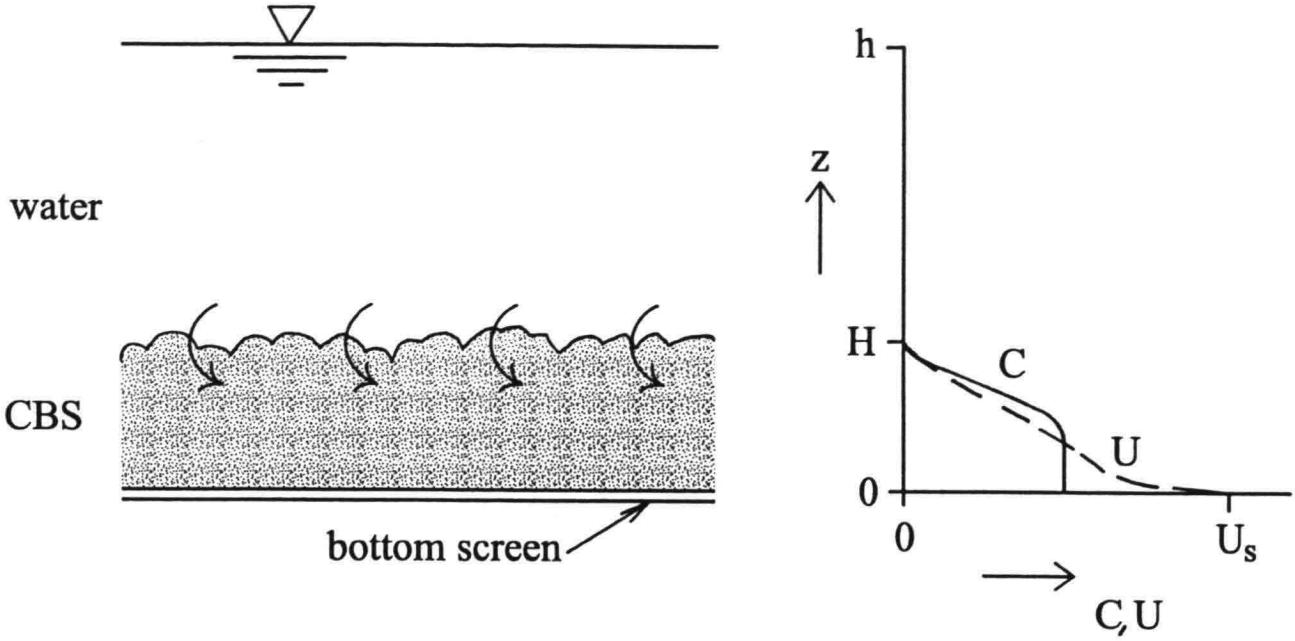

Figure 1. Entraining flow of a CBS layer. A bottom screen drives the flow and produces turbulence. The curved arrows indicate the engulfment of overlying water by the turbulent motions in the CBS layer. The lutocline given by z = H(t) moves upward. The notation is explained in Section 2.

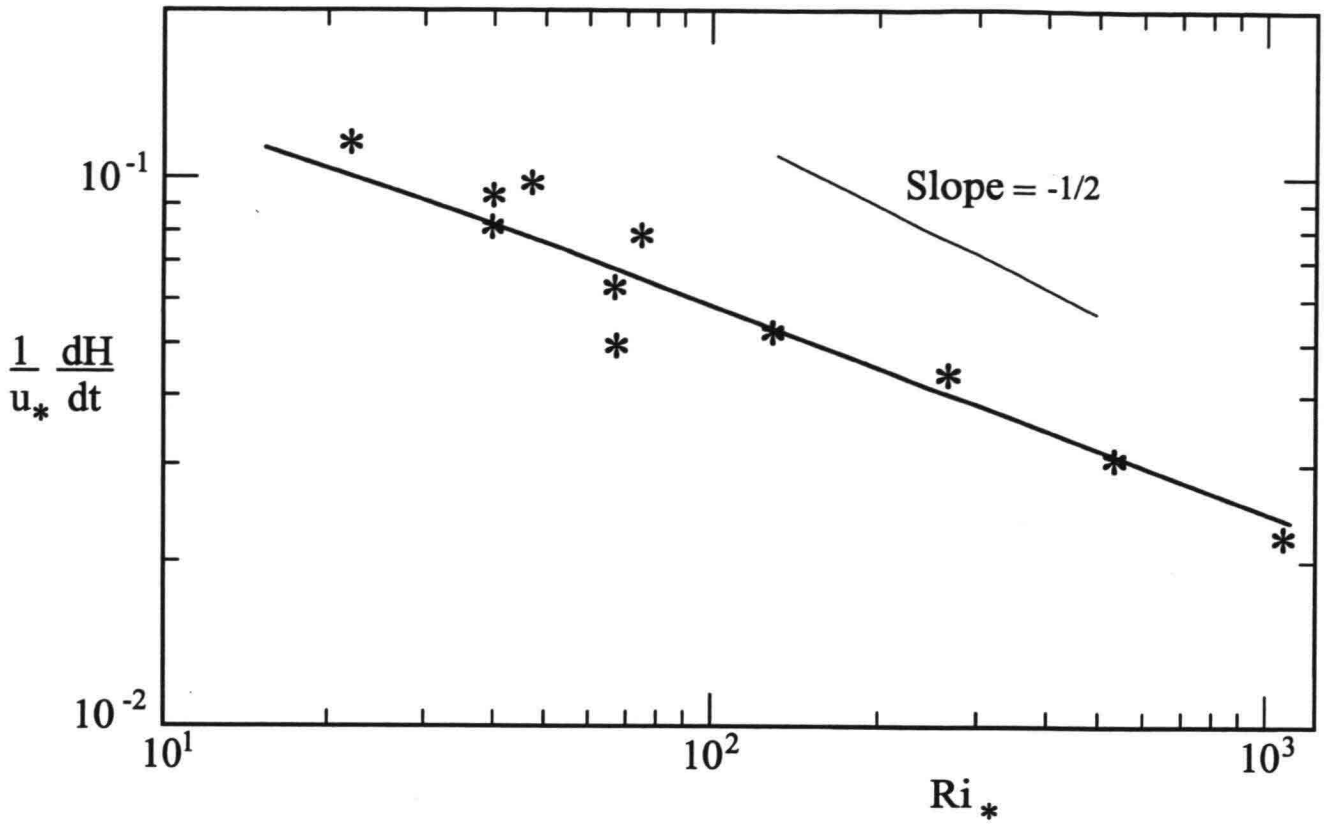

Figure 2. Entrainment rates in a two-fluid system calculated with $\alpha = 12$ and $\sigma_T = 1.5$ (solid line). The experimental data indicated by asterisks are taken from Kranenburg (1984).

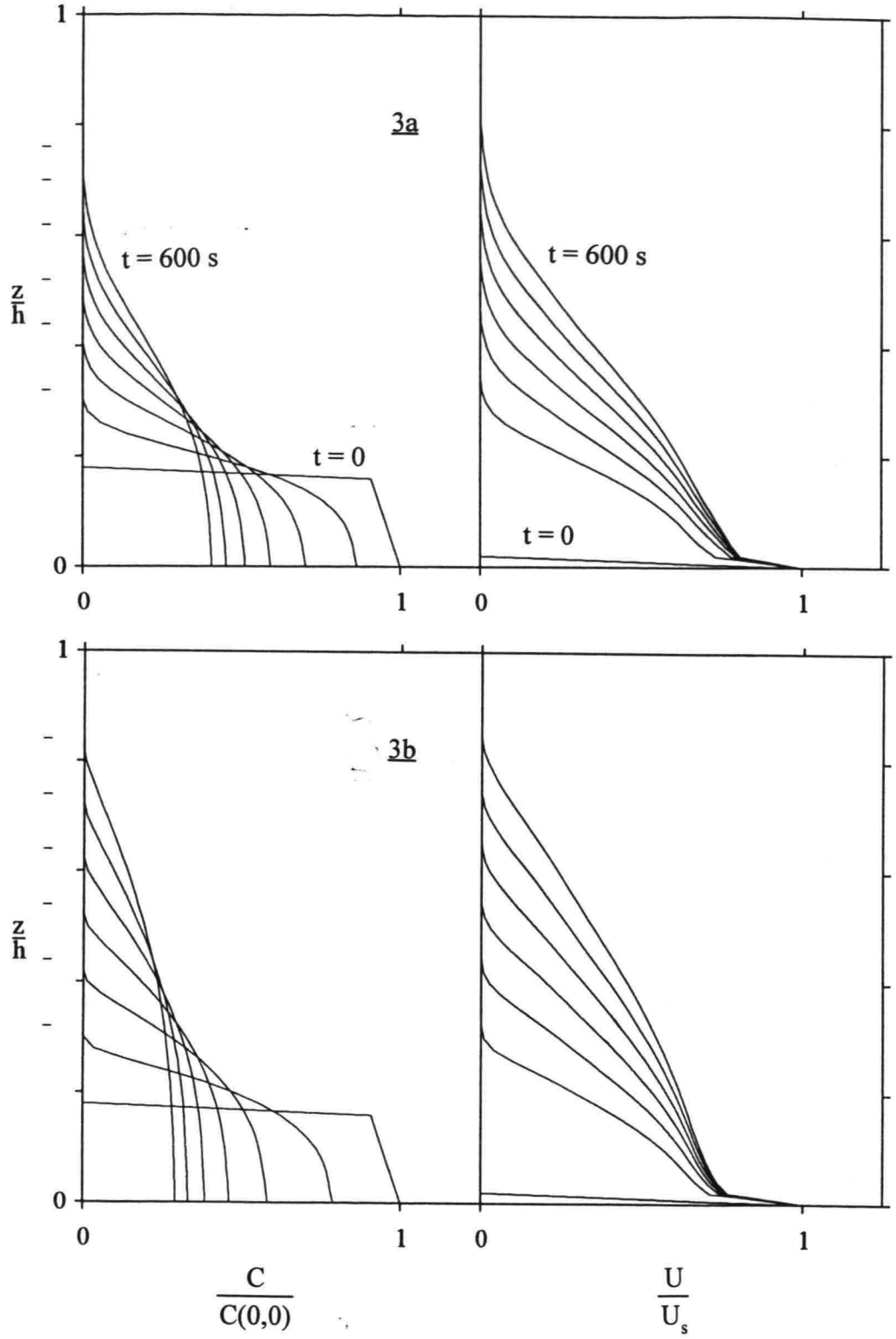

Figure 3. Influence of damping functions and turbulent Prandtl-Schmidt number on calculated concentration and velocity distributions in a two-fluid system. a. Eqs. 2.20 and 2.21, $\sigma_T = 1.5$ (the final value of Ri_* is 630), b. Eqs. 2.20 and 2.21, $\sigma_T = 1$ (the final value of Ri_* is 500), c. Eqs. 2.18 and 2.19, $\sigma_{T0} = 0.7$. The time interval between plots is 100 s. The total simulation time is 600 s. The horizontal dashes on the left of the vertical axes indicate the depths of the CBS layer at the times the distributions are plotted. For Figure 3c see next page.

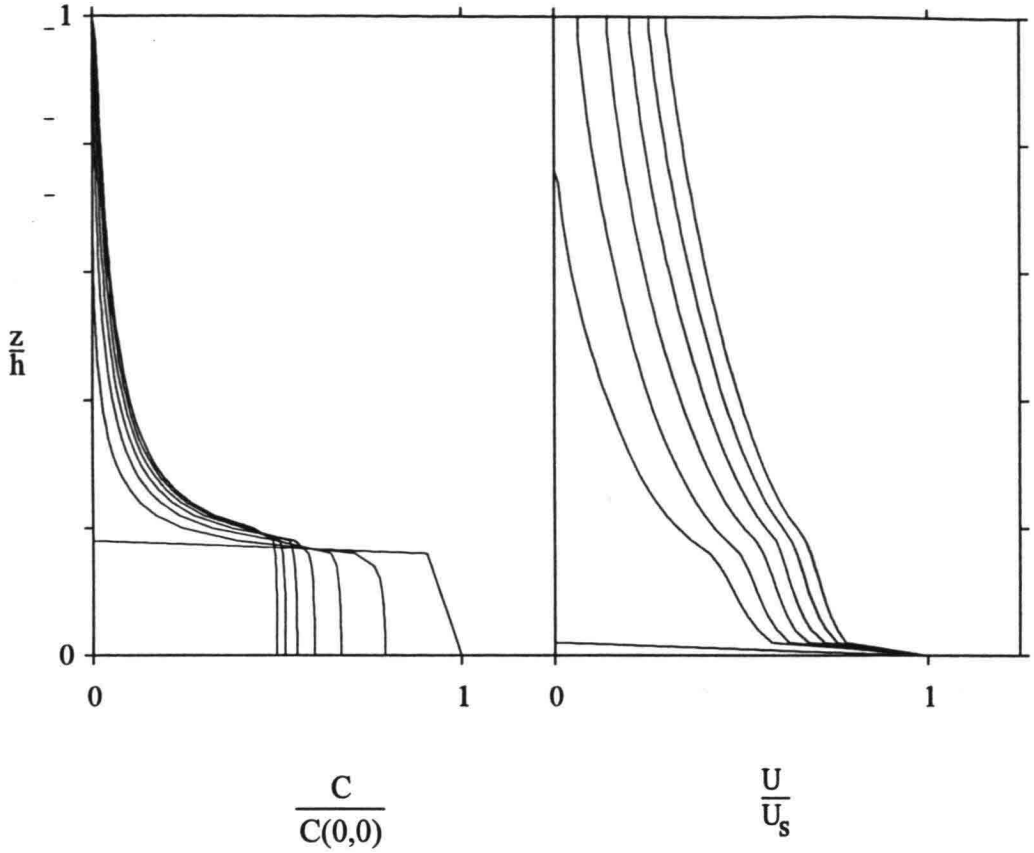

Figure 3c. For caption see previous page.

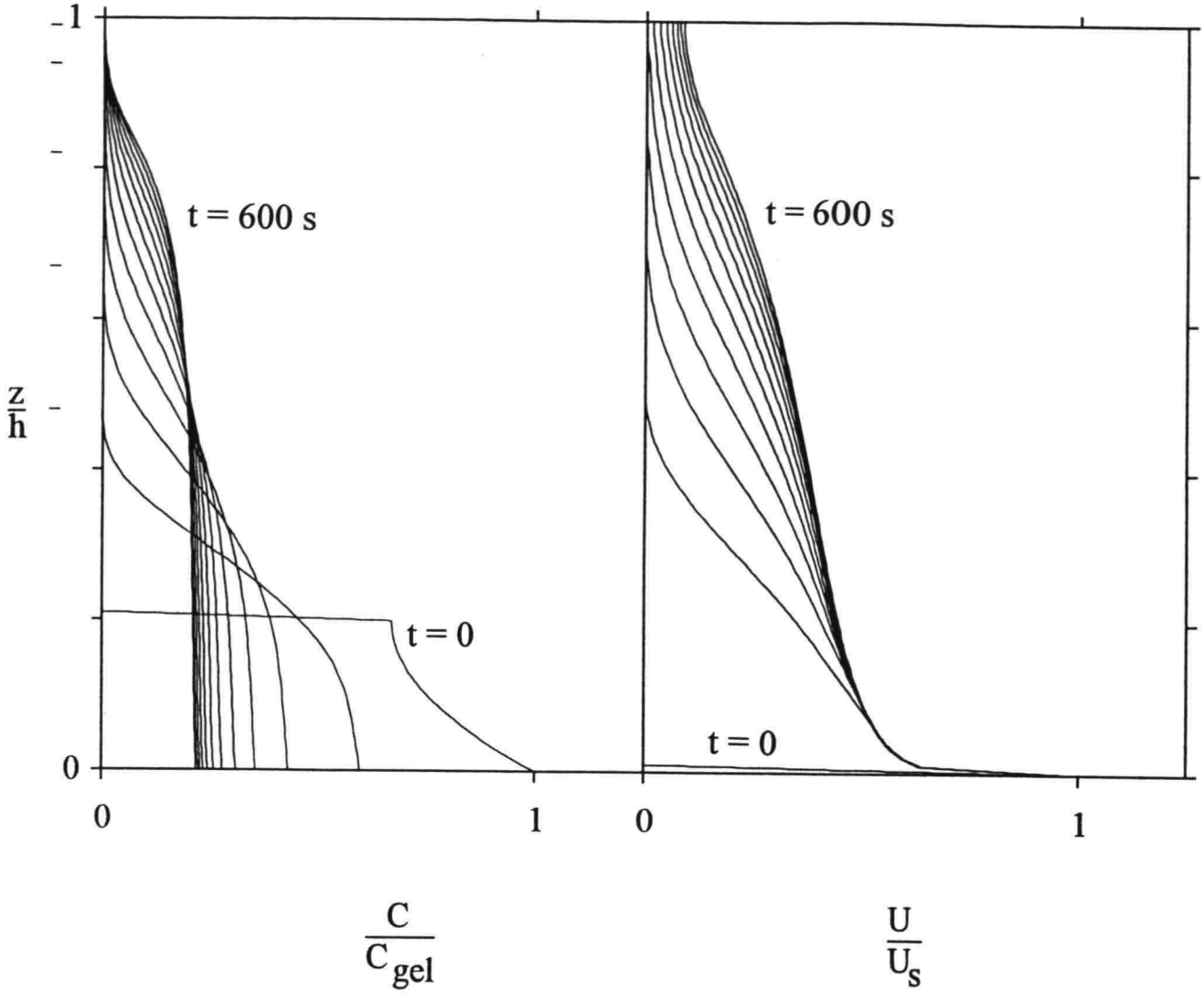

Figure 4. Concentration and velocity distributions for Run 1. The time interval between plots is 50 s. The total simulation time is 600 s.

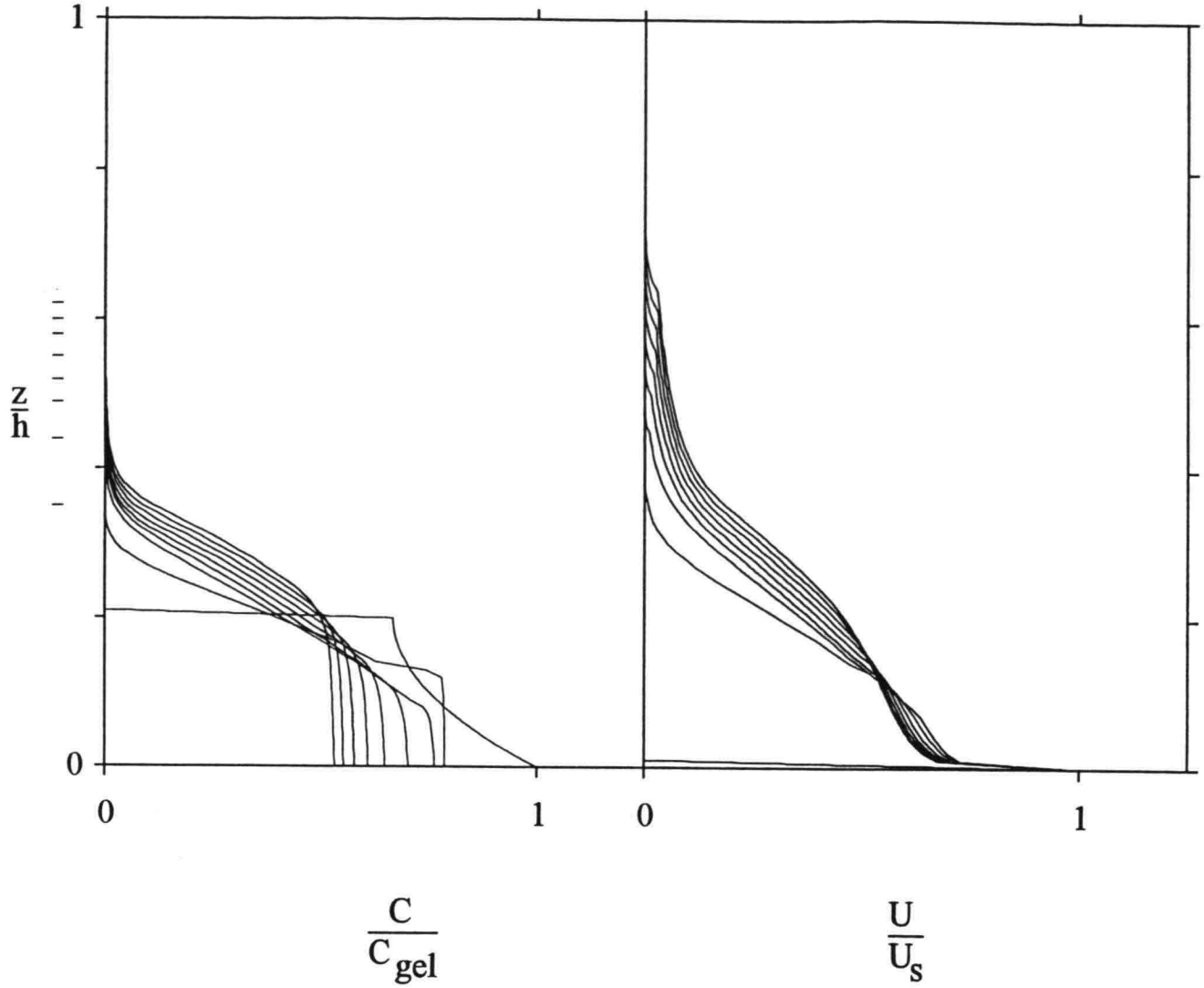

Figure 5. Concentration and velocity distributions for Run 2. The time interval between plots is 50 s. The total simulation time is 400 s.

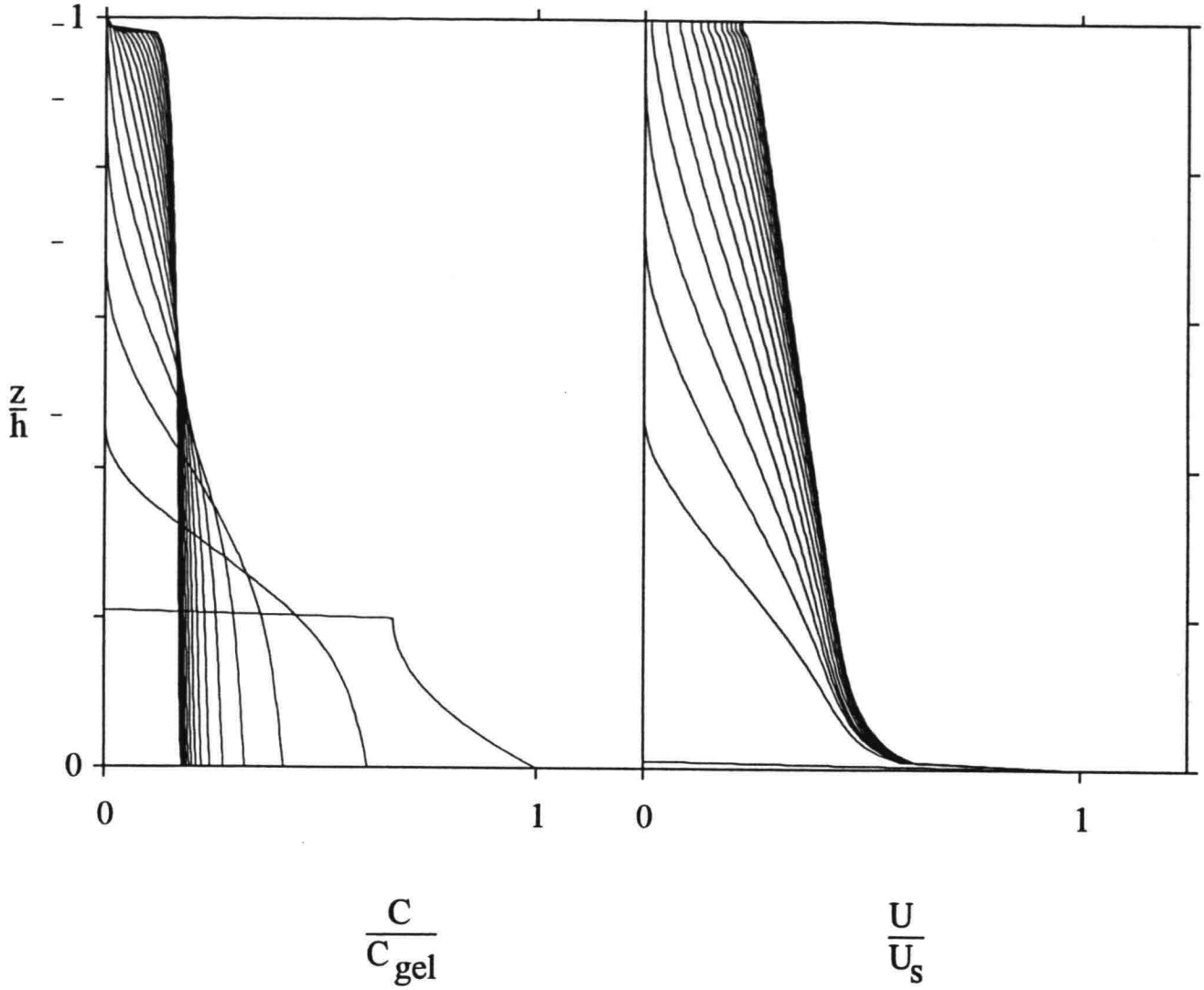

Figure 6. Concentration and velocity distributions for Run 3. The time interval between plots is 25 s. The total simulation time is 400 s.

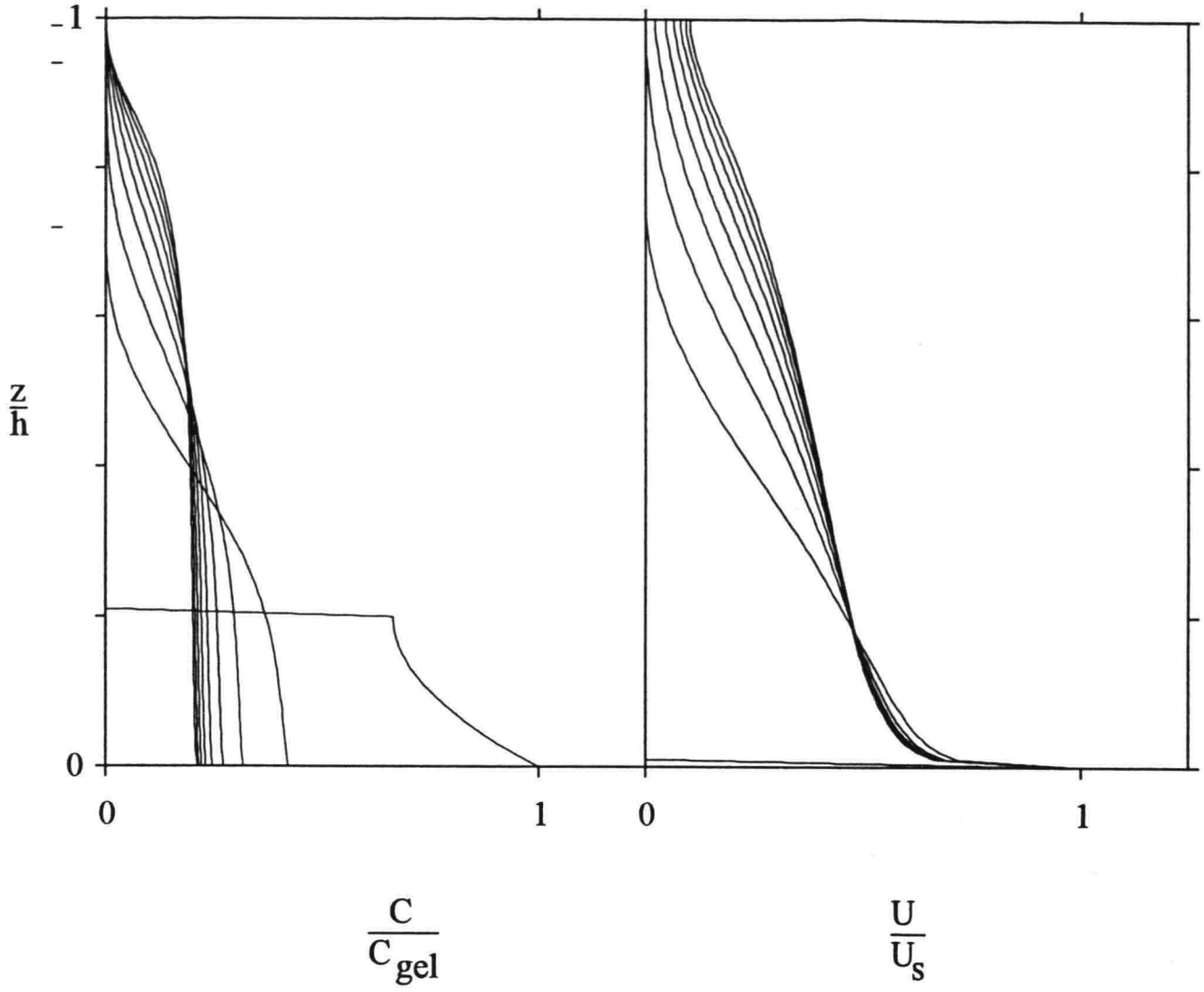

Figure 7. Concentration and velocity distributions for Run 4. The time interval between plots is 50 s. The total simulation time is 400 s.

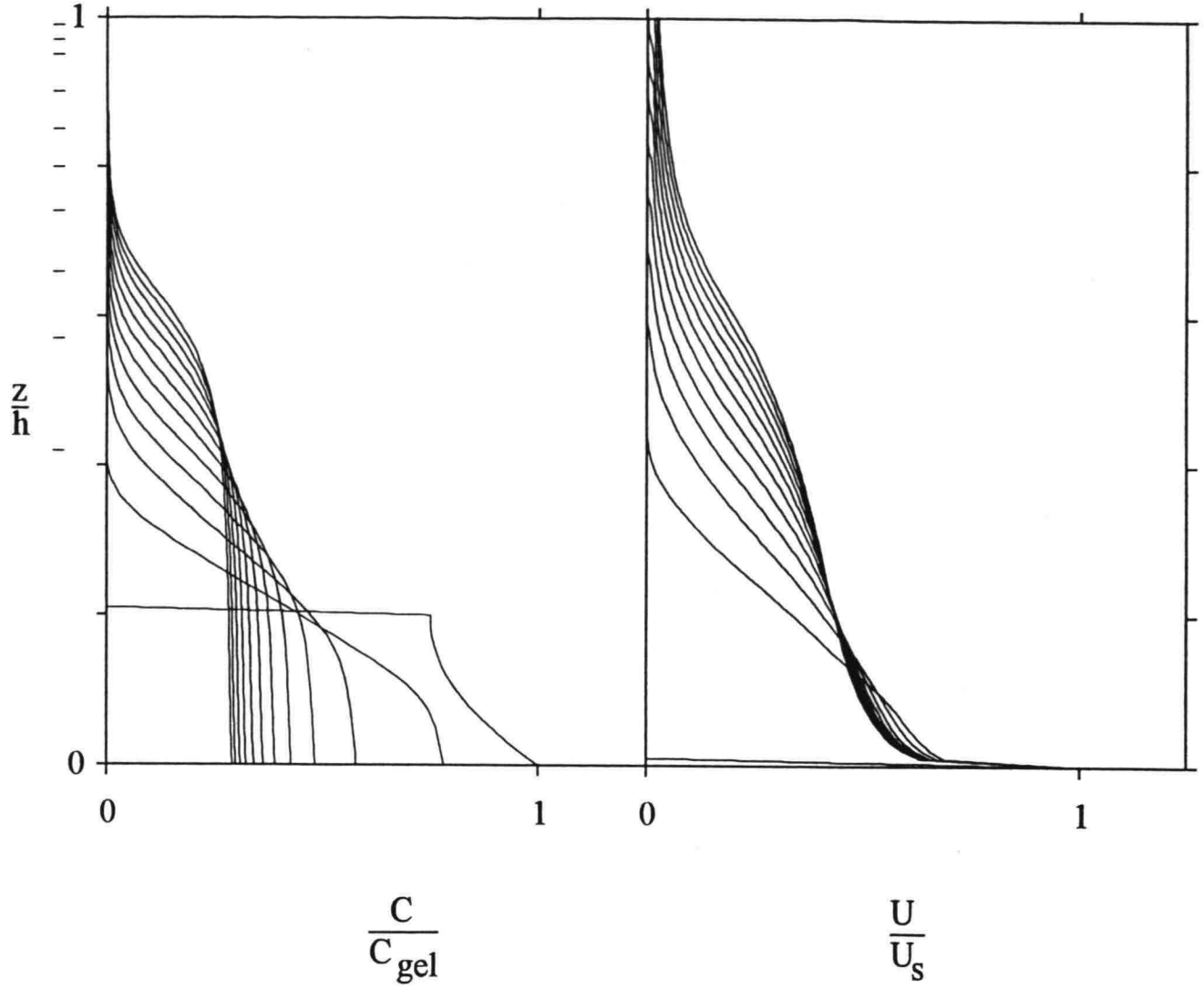

Figure 8. Concentration and velocity distributions for Run 5. The time interval between plots is 50 s. The total simulation time is 600 s.

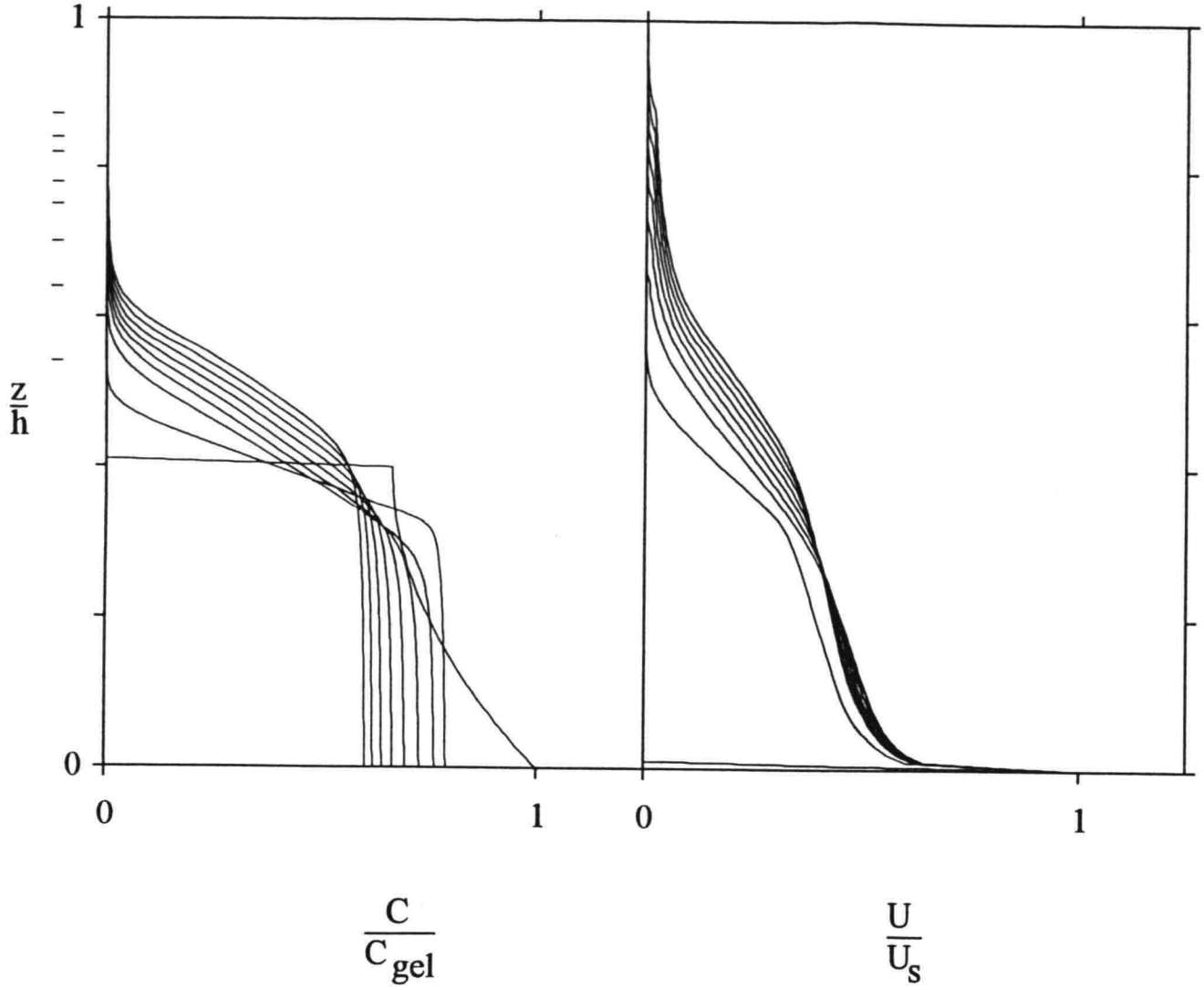

Figure 9. Concentration and velocity distributions for Run 6. The time interval between plots is 50 s. The total simulation time is 400 s.